TROPICAL CYCLONE RESEARCH REPORT
TCRR **1**: 1–14 (2025)
Meteorological Institute
Ludwig Maximilians University of Munich

Towards understanding the tropical cyclone life cycle

Roger K. Smith[a 1] and Michael T. Montgomery[b]
[a] *Meteorological Institute, Ludwig-Maximilians-Universität in Munich, Germany*
[b] *Dept. of Meteorology, Naval Postgraduate School, Monterey, CA, USA*

Abstract:
Conceptual frameworks are discussed for understanding the physics of the tropical cyclone life cycle in an idealized, three-dimensional, numerical simulation in a quiescent environment. Both axisymmetric and three-dimensional frameworks are discussed, a central feature of the former being the assumption that absolute angular momentum is materially conserved above the frictional boundary layer, at least in the classical Eliassen balance formulation. Such conservation implies that vortex spin up requires radial inflow above the friction layer, while radial outflow there leads to spin down. Many of the ideas are illustrated by two simple laboratory experiments.
In contrast, in the axisymmetric WISHE models, the material conservation of absolute angular momentum is disregarded in favour of assuming that the saturated moist equivalent potential vorticity is everywhere zero. This assumption limits the applicability of these models at best to a small portion of the storm's life cycle, even if one were able to justify the implicit angular momentum source thereby introduced. Analysis of a recent three-dimensional numerical simulation of the tropical cyclone life cycle unveils a causality problem with the assumptions underlying these models.
In a three-dimensional framework, the rotating-convection paradigm highlights the importance for vortex spin up of the deep, convectively-induced overturning circulation being strong enough to generate inflow above the frictional boundary layer in the presence of the ubiquitous tendency of the boundary layer to generate outflow there. When deep convection is too weak to ventilate all the mass that is converging in the boundary layer to the upper troposphere, there is net outflow above the boundary layer and the vortex weakens. This behaviour appears to be ruled out in the WISHE models by their assumption of global moist neutrality, but is a feature of the classical Eliassen model.

KEY WORDS Tropical cyclone life cycle; classical intensification models; WISHE intensification models, rotating-convection paradigm

Date: January 3, 2025; Revised ; Accepted

1 Introduction

Tropical cyclones are a regularly occurring natural phenomena threatening life and property in certain regions of the world. Whereas forecasts of their occurrence and tracks have improved significantly in the last two decades, some aspects continue to prove a challenge to forecasters, such as when storms develop or decay rapidly as they approach landfall. A case in point was Hurricane Otis (2023) that developed rapidly when it was close to the Mexican city of Acapulco and caused enormous damage to that city as it crossed the coast as a Category 5 storm.

The general improvement of forecasts can be attributed in part to an improvement in numerical forecast models as well as improvements in observational capabilities, especially those linked to satellite surveillance and remote sensing. The improvement of numerical forecast models has come about not only from vastly improved computer facilities available to forecast centres, but also to advances in understanding many aspects of tropical cyclone behaviour (e.g., Zhang et al. 2015; Zhu et al. 2021).

[1]Correspondence to: Prof. Roger K. Smith, Meteorological Institute, Ludwig-Maximilians University of Munich, Theresienstr. 37, 80333 Munich. E-mail: roger.smith@lmu.de

In this short essay we review some of the key theoretical advances that have taken place in the last few decades and go on to identify areas where more research is called for. One particular aim is to assess the applicability of two old, but still prominent axisymmetric theories (Section 2) to understand the tropical cyclone life cycle. A further aim is to review a more recent paradigm that we have developed (Smith and Montgomery 2023, Chapter 11). This paradigm appears to be a useful framework for understanding both axisymmetric and asymmetric aspects of vortex evolution.

2 Axisymmetric models

Although tropical cyclones only become approximately axisymmetric as they mature, and only then in their inner core region (Smith and Montgomery 2023, Chapter 4), axisymmetric models would seem to be a good place to start in trying to understand their dynamics. Here we review two such models: what we shall call the classical model that emerges from the work of Willoughby (1979), Shapiro and Willoughby (1982), and Schubert and Hack (1982, 1983); and what we will refer to as the WISHE models that are based on the work of Emanuel (1989, 1995, 1997, 2012). In a recent paper, Smith et al. (2024)

sought to relate the dynamics of these theories, but found some fundamental differences in the two formulations. These differences are discussed in Section 2.5.

2.1 Material conservation of M

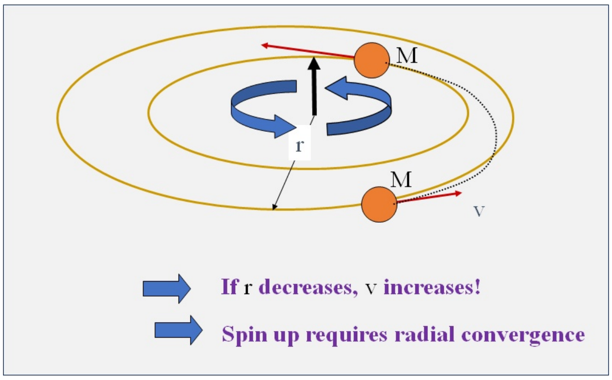

Figure 1. Illustration of the amplification of the tangential velocity in an axisymmetric vortex as a result of radial inflow and the conservation of M. See text for further discussion.

A key concept for understanding the spin up of an axisymmetric vortex is the material conservation of the absolute angular momentum, M, above the frictional boundary layer. The quantity is defined in terms of the tangential velocity, v, the radius from the rotation axis, r, and the Coriolis parameter f, assumed to be constant[1] by the relationship

$$M = rv + \frac{1}{2}fr^2. \qquad (1)$$

Referring to an air parcel moving in an inward-spiralling path where there is no frictional stress in the tangential direction, the material conservation of M for that parcel implies that the tangential wind speed will increase (Figure 1). Conversely, if the parcel were spiralling outwards, the tangential wind speed will decrease, possibly changing sign if the radial displacement is large enough. We may conclude that spin up of the tangential wind requires radial inflow and that radial outflow leads to spin down. The material conservation of M follows directly from the tangential momentum equation when there are no frictional or sub-grid scale forces in the azimuthal direction (see Smith and Montgomery 2023, Section 5.6).

2.2 Two insightful laboratory experiments

In general, *there are two fundamental requirements for vortex amplification: a source of rotation and some forcing mechanism to concentrate the rotation*. The interplay between the strength of the forcing and that of rotation can be illustrated by the first of two elementary fluid experiments. These experiments, shown in Fig. 2, are useful for illustrating two important elements of understanding tropical cyclone evolution: the roles of deep convection and the frictional boundary layer.

[1] If f were not constant, the flow could not be axisymmetric.

2.2.1 The role of convection

In the first experiment, due to Turner and Lilly (1963), a vortex is produced in water contained in a rotating cylinder by releasing bubbles from a thin tube along the upper part of the rotation axis. As the bubbles rise, they exert a drag on the water which forces an overturning circulation with radial inflow below the bubbling tube and radial outflow above. The drag exerted by the bubbles is analogous to the effect of cloud buoyancy in the atmosphere.

Except in a shallow boundary layer near the lower boundary, converging rings of water conserve their absolute angular momentum and consequently spin faster as they are drawn inwards toward the axis of rotation. The ultimate degree of amplification of the angular velocity depends on how far rings of fluid can be drawn inwards by the overturning circulation produced by the rising bubbles. This inward displacement increases with the bubbling rate, but decreases with increasing background rotation rate.

If the forcing is sufficiently large for a given rotation rate, rings of fluid may be drawn in to relatively small radii before the sum C of the centrifugal force per unit mass

$$\mathrm{CEN} = \frac{v^2}{r} \qquad (2)$$

and Coriolis force per unit mass

$$\mathrm{COR} = 2\Omega v \qquad (3)$$

opposing the inward motion balance the radial pressure gradient force per unit mass

$$\mathrm{PGF} = -\frac{1}{\rho}\frac{\partial p}{\partial r} \qquad (4)$$

induced by the bubbles. It is this pressure gradient force that drives the rings of fluid inwards (middle panel of Fig. 2). Again, v is the azimuthal velocity component and r is the radius from the rotation axis. In addition, f, now equal to 2Ω, is twice the background rotation rate of the cylinder, p is the pressure and ρ is the density of water.

If the forcing is comparatively weak, or if the rotation rate is sufficiently strong, a balance of the radial forces may be achieved before the radial displacement of a fluid parcel is very large, so that a significant amplification of the background rotation will not be attained. Clearly, if there is no background rotation, there will be no amplification, and if the background rotation is very weak, the centrifugal and/or Coriolis forces never become large enough to balance the radial pressure gradient, except possibly at large radii from the source of bubbles. *This reasoning points to the existence of an optimum*

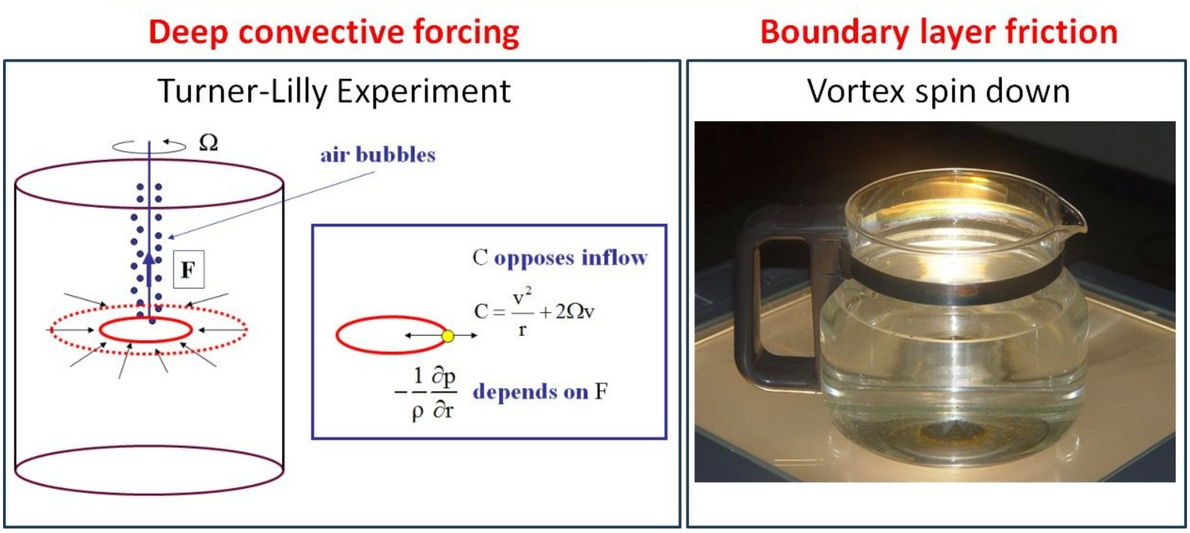

Figure 2. Left: Schematic of flow configuration in the Turner and Lilly experiment. The right side indicates the principal forces per unit mass acting on an air parcel in the radial direction: an inward-directed pressure gradient force, $-(1/\rho)(\partial p/\partial r)$, and an outward force C, the radial component of generalized Coriolis force, which is the sum of the centrifugal force (v^2/r) and Coriolis force $(2\Omega v)$. Right: The tea-leaves experiment showing the effects of frictionally-driven inflow near the bottom after the water has been stirred to produce rotation. This inflow carries tea leaves to form a neat pile near the axis of rotation.

forcing strength to produce the maximum amplification of the tangential velocity for a given strength of background rotation, or an optimum background rotation rate for a given forcing strength as eloquently articulated by Morton (1966). These ideas were demonstrated in related numerical experiments in the context of thermally-driven vortices by Smith and Leslie (1976).

The foregoing arguments emphasize the unbalanced wind adjustment from the instant that the bubbling is turned on, in contrast to the more gradual adjustments that occur typically in tropical cyclones. In fact, the bubbling experiment was originally conceived as one for demonstrating how a tornado vortex might descend from a cloud (Morton 1966). Nevertheless, if the container is relatively wide and shallow and the bubbles are generated over the layer from a ring of tubes, the experiment should be relevant to understanding tropical cyclones also, especially when a vortex has become established at the surface. In particular, as discussed later, the experiment allows one to consider the evolution of the vortex when the bubbling rate is slowly varied, analogous to changes in convective activity in a real storm.

When a concentrated vortex has formed and extended to the lower boundary, frictional effects become important. These may be illustrated by a second experiment that can be easily carried out in the home (right panel of Fig. 2).

2.2.2 The frictional boundary layer

The classical spin down problem for a vortex considers the evolution of an axisymmetric vortex above a rigid boundary normal to the axis of rotation. The spin down is primarily a result of the tangential component of generalized Coriolis force per unit mass, $-u(v/r + f)$, which depends on the secondary circulation induced by friction above the boundary layer. The direct effect of the frictional diffusion of tangential momentum *to* the surface with frictional drag *at* the surface are of secondary importance to the spin down in the parameter regimes relevant to tropical cyclones.

One can demonstrate the frictionally-driven inflow simply by placing tea leaves in a water container and vigorously stirring the water to set it in rotation. After a short time, the tea leaves congregate in a neat pile at the bottom of the container near the axis, as shown in right panel of Fig. 2. They are swept there by the inflow in the friction layer. Slowly, the rotation in the container declines because the inflow towards the rotation axis in the friction layer has to be accompanied by radially-outward motion in the vortex above this layer in order to satisfy mass continuity.

The depth of the friction layer depends on the viscosity of the water and the rotation rate of the water and is typically only on the order of a millimeter or two in this experiment. Because the water is rotating about the vertical axis, it possesses angular momentum about this axis. Here, because the container, itself, is not rotating, angular momentum, M, is defined as the product of the tangential flow speed and the radius.

2.2.3 Insights from these laboratory experiments

In conjunction with the tea-leaves experiment, the Turner-Lilly bubbling experiment helps illustrate an important aspect of tropical cyclone behaviour when tropical cyclones approach maturity and deep convection

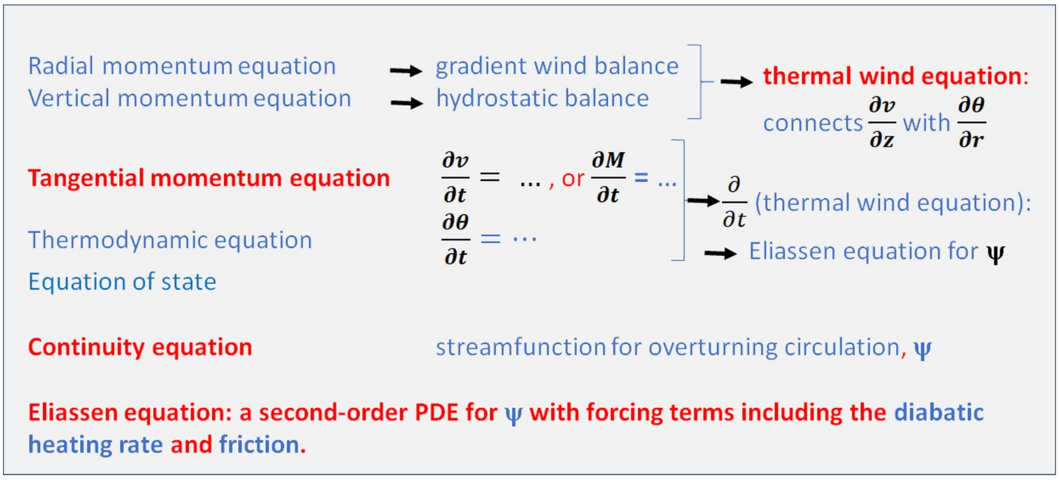

Figure 3. Schematic of the axisymmetric balance equations for tropical cyclone intensification. The equations in red are the ones used in a prognostic theory. See text for discussion.

becomes progressively unable to ventilate all the air that is converging in the frictional boundary layer (see Section 3.1). This scenario may be imagined in the context of the bubbling experiment. When a steady-state vortex had emerged in that experiment, the deep overturning circulation produced by the drag of the rising bubbles will be fed by the water converging in the frictional boundary layer. Imagine then what happens if the bubbling rate is slowly reduced. In that case, the divergence induced by the boundary layer above the boundary layer will be stronger than the bubbling-induced circulation can support, leading to net outflow above the boundary layer and vortex spin down there on account of the material conservation of M. We can imagine the formation of a weaker and broader vortex to emerge if the bubbling rate becomes steady at a lower rate than before. An analogous behaviour is found during the tropical cyclone life cycle as discussed in Section 4.

2.3 The classical balance model

The classical model for tropical cyclone intensification is built on the seminal studies of the thermally or frictionally-controlled meridional circulation in a circular vortex and of frontal circulations by Eliassen (1951, 1962). Similar formulations for the diagnosis and evolution of the balanced tangential and overturning circulation of an idealized axisymmetric tropical cyclone were developed by Willoughby (1979), Shapiro and Willoughby (1982), Schubert and Hack (1982, 1983) and Schubert and Alworth (1982). *The underlying premise of these classical models, supported by a scale analysis of the governing equations, is that the cyclone remains in hydrostatic and gradient wind balance as it evolves.* With this assumption, one obtains a linear second-order partial differential equation for the streamfunction of the overturning circulation, forced by prescribed heat and tangential momentum sources. Without such a circulation, these sources would act immediately to destroy balance. The equation is commonly referred to as the *Eliassen equation*[2]. The axisymmetric equations underlying the classical model formulations as well a supporting scale analysis are detailed in Smith and Montgomery (2023) (Chapters 5, 8 and Sections 16.1.8 and 16.1.9) and summarized schematically in Fig. 3. In essence, the classical models are incorporated in the cooperative intensification theory of Ooyama (1982).

2.3.1 The axisymmetric balance equations

The axisymmetric balance model is based on the momentum equations for the radial, u, vertical, w, and tangential, v, velocity components, a thermodynamic equation for the potential temperature[3], θ, an equation of state, and a mass continuity equation for the transverse circulation. The radial and vertical momentum equations are approximated by gradient wind balance and hydrostatic balance, respectively, as justified by a scale analysis. Elimination of the pressure from these two balance equations gives *the thermal wind equation*, which is a diagnostic equation relating the vertical gradient of tangential wind to the radial gradient of potential temperature.

Differentiation of the thermal wind equation partially with respect to time and eliminating the time derivatives using the tangential momentum equation and potential temperature equation gives a diagnostic equation for the transverse, overturning circulation involving u and w. Finally, using the mass continuity equation to introduce a streamfunction, ψ, for the transverse circulation, one ends up with the Eliassen equation, a linear, second-order partial differential equation for ψ at any given time.

[2] Sometimes referred to also as the Sawyer-Eliassen equation.
[3] In actual fact, the inverse of the potential temperature is used.

The reduced set of balance equations, coloured red in Fig. 3, form a prognostic dynamical system that may be solved as follows (Smith et al. 2018):

- Given an initial tangential wind profile as a function of r and z and a sounding of pressure and temperature at some large radius, one can use the thermal wind equation to determine the pressure field (the characteristics of this first-order partial differential equation are just the isobars) and the balanced density and potential temperature fields at the initial time;
- Then, given some distribution of diabatic heating and friction, one can solve the Eliassen equation for $\psi(r, z)$, from which the radial and vertical velocity components can be obtained;
- Finally, the tangential momentum equation can be applied to advance the solution in time, and so on.

2.3.2 Some solutions: inviscid case

The solution character in a typical prognostic calculation of the classical balance theory is exemplified by the flow configuration in Fig. 4. In this case, the flow is taken to be inviscid and the distribution of diabatic heating rate, $\dot{\theta}$, is prescribed relative to M-surfaces that slope outwards with height and, for an inertially stable vortex, M increases with radius, Typical distributions of $\dot{\theta}$ associated with deep convection have a maximum in the low to middle troposphere, well above the top of the boundary layer (Montgomery et al. 2006, Fig. 6d; Bui et al. 2009, Fig. 3a,c; Smith et al. 2014, Fig. 7a,b; Črnivec et al. 2015, Fig. 6a-c). A key feature to note is the structure of the overturning circulation with inflow in the lower troposphere and outflow in the upper troposphere. The ascent region is confined to the region of heating with the maximum ascent close to the level of maximum diabatic heating rate.

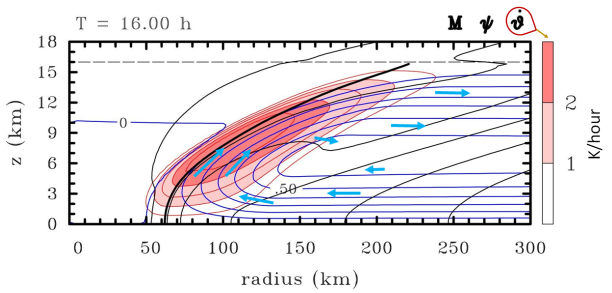

Figure 4. Radius–height cross sections of M surfaces (black curves) superimposed on the streamlines of the secondary circulation, ψ, (blue curves) and diabatic heating rate, $\dot{\theta}$ (shaded), but no friction in the calculation described in the text. From Smith et al. (2018).

Note that the streamlines generally cross the M-surfaces in the lower troposphere in the direction of diminishing M. Thus, invoking the principle of material conservation of absolute angular momentum, M (Section 2.1), the M-surfaces will be advected inwards there and the tangential velocity will increase. In the upper troposphere, the M-surfaces will be advected outwards and the tangential velocity will decrease and eventually reverse direction to become anticyclonic.

2.3.3 Some solutions: friction only case

An example of the friction only case is shown in Fig. 5. In this case, the parametrerized frictional forcing in the Eliassen equation is specified in a shallow surface-based layer on the order of a kilometre deep. In response, there is radial inflow in the friction layer and radial outflow just above it. As in the tea-leaves experiment in Fig. 2, the radial outflow advects M-surfaces outwards leading to a progressive spin down of the tangential velocity in the outflow layer. In contrast to the situation in the tea-leaves experiment, the outflow is vertically confined to a relatively shallow layer on account of the static stability of the flow.

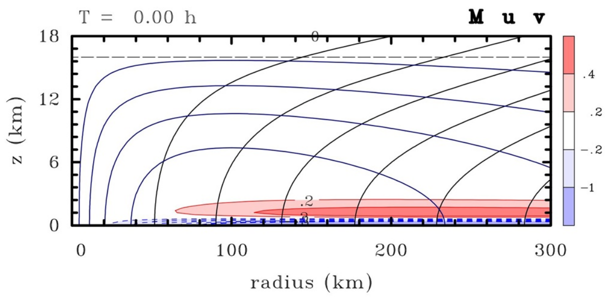

Figure 5. Radius–height cross sections of M-surfaces (black curves) superimposed on the contours of radial velocity, u (shaded) and tangential velocity, v (blue curves) at the initial time in the calculation with friction, but no diabatic heating, described in the text. At later times, the pattern retains a similar structure, but with the location of maximum v becoming elevated and both flow components weakening. For further details, see Smith et al. (2018), Section 2d.

2.3.4 Some solutions: heating and friction case

Combining the heating only and friction only cases discussed above, it is easy to see what to expect in the case with friction and heating. Note that the Eliassen equation is linear so that the separate effects of heating and friction on the secondary circulation, ψ, are adddi-tive. Friction has the persistent effect to advect the M-surfaces outwards above the boundary layer leading to spin down. Clearly, for the tangential wind speed to spin up, the diabatic heating rate and its spatial distribution must be strong enough to reverse the frictionally-driven outflow, thereby enabling the M-surfaces to be advected inwards. In the balance model, the boundary layer spin-up enhancement mechanism, described by Smith and Montgomery 2023, Section 2.3.4, does not operate.

2.4 Summary

In summary, the classical intensification models capture many observed features of an intensifying storm.

- They capture inflow in the lower troposphere and outflow in the upper troposphere;
- They capture ascent in the region of heating, with a vertical velocity maximum in the middle troposphere;
- They capture the spin up of the vortex in the lower troposphere;
- They capture the formation of an anticyclone in the upper troposphere;
- If the diabatic heating is too weak, they show shallow outflow above the friction layer and spin down. This behaviour is analogous to vortex spin down in the Turner-Lilly bubbling experiment when the bubbling rate is reduced (see Section 2.2.3).

These models are clearly useful for understanding important aspects of how storms intensify and decay. However, they do not provide a physically closed theory because of the need to specify the diabatic heating rate associated with deep convection as a function of space and time. Moist processes are implicit in this specification, which is a clear limitation of the models' applicability to more realistic situations. This limitation notwithstanding, if the diabatic heating rate distribution can be deduced from observations or numerical solutions, the models may be used in a diagnostic sense to estimate the tendencies of the balance flow.

Ideally, moist processes should be considered explicitly as part of the problem. A recent attempt to do this within a balance framework was unsuccessful, although it did highlight two important findings (Smith et al. 2024).

1. As soon as convective instability occurs in the model, the Eliassen equation becomes non-elliptic and cannot be solved without some ad hoc procedure to "regularize" the equation in these regions (e.g., Bui et al. 2009, Wang and Smith 2019, Montgomery and Persing 2020, Wang et al. 2021). However, such "regularization" leads to moist neutral ascent, removing the capability of the diabatic heating distribution to draw M-surfaces inwards above the boundary layer.

2. The only way to remove this limitation is to apply a suitable parameterization of deep convection that does produce inflow above the boundary layer, allowing the M-surfaces to be drawn inwards there.

An effort to develop a physically closed theory is examined in the next section.

2.5 WISHE models

The flow configuration of the axisymmetric WISHE models referred to in Section 2 is summarized in Fig. 6. The overturning circulation is inwards only in a shallow friction layer and it is upwards and outwards above the friction layer. The key assumption is that the M-surfaces are congruent with those of saturation equivalent potential temperature θ_e^* so that the saturation moist potential vorticity, say P_m, is everywhere zero[4]. The mathematical definition of P_m is

$$P_m = \frac{\boldsymbol{\omega_a} \cdot \nabla\theta_e^*}{\rho} \tag{5}$$

where $\boldsymbol{\omega_a}$ denotes the absolute vorticity in the traditional formulation (i.e., $\boldsymbol{\omega_a} = f\hat{\mathbf{k}} + \nabla \wedge \mathbf{u}$ and $\hat{\mathbf{k}}$ the vertical unit vector), ρ is the density and $\mathbf{u}$ is the relative velocity field vector[5]. It is assumed further that θ_e^*, is equal the subcloud layer equivalent potential temperature, θ_e, where an air parcel emerges from the boundary layer.

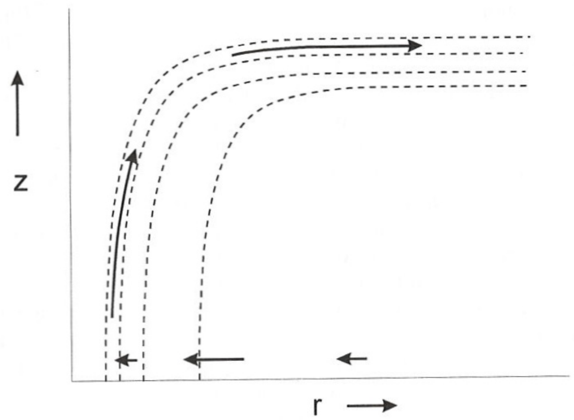

Figure 6. The WISHE view of tropical cyclone physics according to Emanuel (2000). The dashed lines indicate surfaces of constant saturation equivalent potential temperature θ_e^*, a quantity that is tied to the subcloud layer equivalent potential temperature, θ_e. Emanuel notes that "the core is warm because surface fluxes have increased θ_e there. The rate of intensification is limited by the surface fluxes, not by the convection, which is very fast by comparison. Intensification stops when the frictionally-induced radial advection of low θ_e air balances the surface enthalpy flux." Reproduced with permission of Academic Press.

Significantly, the flow indicated in Fig. 6 is radially outward above the friction layer, as in the classical model

[4]It may be worth noting that the assumption that P_m is everywhere zero implies that the moist Eliassen equation is not elliptic. This condition implies also moist neutrality in the sense that a small air parcel displacement along an M-surface is neutral.

[5]P_m may be expressed equivalently as

$$P_m = \frac{\hat{\mathbf{j}}}{r\rho} \cdot \nabla\theta_e^* \wedge \nabla M \tag{6}$$

with $\hat{\mathbf{j}}$ denoting the unit vector in the azimuthal direction.

with friction only: see e.g., Fig. 5. With this flow configuration, the vortex in the classical model spins down as M surfaces are carried outwards above the boundary layer. Moreover, the maximum vertical velocity w_{max} is at the top of the boundary layer. Recognition of these features raises the question: how does spin up occur in the WISHE models in the presence of outflow above the boundary layer? We address this question in the next subsection.

2.5.1 Spin up in the WISHE models

It should be noted that the assumption of zero P_m does not, by itself, guarantee the material conservation of M above the boundary layer[6]. In contrast to the classical models discussed above, nowhere in the WISHE models does the material conservation of M seem to be *imposed* above the boundary layer. This is certainly the case in the 1997 and 2012 formulations. In these cases, there must be a source of M that enables the M-surfaces to move inwards above the boundary layer in the presence of outflow there. In this sense, the WISHE models cannot be considered as physically closed. Whether or not the distribution of these sources or sinks is in any sense realistic remains an open question and to our knowledge, the distribution of the angular momentum source/sink in these models has never been shown. In Appendix 1 of Smith et al. (2024), it is shown that the material source of M may be diagnosed as

$$\frac{DM}{Dt} = \frac{\partial M}{\partial \theta_e^*}\frac{D\theta_e^*}{Dt} + \left.\frac{\partial M}{\partial t}\right|_{\theta_e^*}, \qquad (7)$$

once the solution for M and θ_e^* has been determined. The material derivative is defined by $D/Dt = \partial/\partial t + u\partial/\partial r + w\partial/\partial z$.

2.5.2 Can one justify the assumption of congruence?

Figure 7 shows an azimuthal analysis of the moist isentropes and M-surfaces taken from a recent idealized, three-dimensional, numerical simulation of a tropical cyclone life cycle (Smith et al. 2021). This simulation is described briefly in Section 4. In particular, the intensity of the simulated cyclone, characterized here by the maximum azimuthally-averaged tangential wind speed, V_{max}, is shown in Fig. 9. It is of interest to examine at what stage, if any, the azimuthally-averaged M- and θ_e^*-surfaces become appreciably congruent in a simulation that explicitly represents rotating deep convective clouds. Although this would seem to be a reasonable task to address, subtleties arise in such an endeavour.

[6]This is because zero potential vorticity simply implies that the M surfaces must be always congruent to the saturated equivalent potential temperature surfaces. However, in general, the M-surfaces can move relative to the θ_e^*-surfaces. In other words, the congruence assumption implies only that $M = M(\theta_e^*, t)$, where t is the time, and is not a function of θ_e^* alone.

The air ascending in the developing eyewall of a simulated axisymmetric vortex is necessarily saturated and to a good first approximation, neglecting the effects of subgrid-scale diffusion, θ_e^* is materially conserved. In contrast, in a non-axisymmetric vortex, the air in the developing eyewall is not necessarily saturated at all azimuthal locations at a particular radius. For this reason, an azimuthal average of θ_e^* seems to be an inappropriate quantity to examine and this average may no longer be materially conserved to as good an approximation as in an axisymmetric configuration. Since in the absence of diffusion, θ_e is materially conserved in both asymmetric and axisymmetric configurations, we would argue that it is the most suitable invariant to assess the possible congruity of M and θ_e in a three-dimensional vortex without ice processes operating.

Figure 7 shows radius-height cross sections of the azimuthally-averaged M- and θ_e-surfaces at 6.5 days, 7.5 days, 8.5 days, 9.5 days, 11 days, and 12.5 days in the life-cycle simulation. Referring to Fig. 9, 6.5 days is about the time when rapid intensification begins. At this stage, congruence is nowhere evident (Fig. 7a). At 7.5 days, which is midway during the period of rapid intensification, the M- and θ_e-surfaces show signs of becoming aligned in the main updraught region in the middle troposphere (Fig. 7b), but not in the lower-to-mid troposphere where the highlighted M surfaces cross many θ_e surfaces. Even in the mature stage, at 8.5 and 9.5 days (Figs. 7c,d), congruence is only approximate in this main updraught region and certainly not interior or exterior to this region. At 11 days (Fig. 7e), which is at a stage where the intensity has weakened somewhat (cf. Fig. 9), the main updraught has weakened also and there is little semblance of congruence even in this region. With some re-intensification, at 12.5 days (Fig. 7f), some degree of congruence has become re-established in the main updraught region, but nowhere else. At later times (not shown), the degree of congruence deteriorates, even in the main updraught region.

Evidently, the assumption that the M- and θ_e-surfaces are congruent does not hold to a plausible degree during intensification in the three-dimensional configuration. Moreover, at the time when rapid intensification begins (about 6.5 days) there is no degree of congruence whatsoever. Notwithstanding the fact that we have shown the azimuthally-averaged θ_e rather than θ_e^*, these results provide little support for one of the cornerstone assumptions on which the time-dependent WISHE models are based. Further, we are unaware of any other contrary analyses supporting the assumption that the M- and θ_e^*-surfaces are globally congruent.

2.5.3 Comparison with observations and numerical simulations

An acid test of any theory is its ability to explain observations and numerical model simulations. The assumed

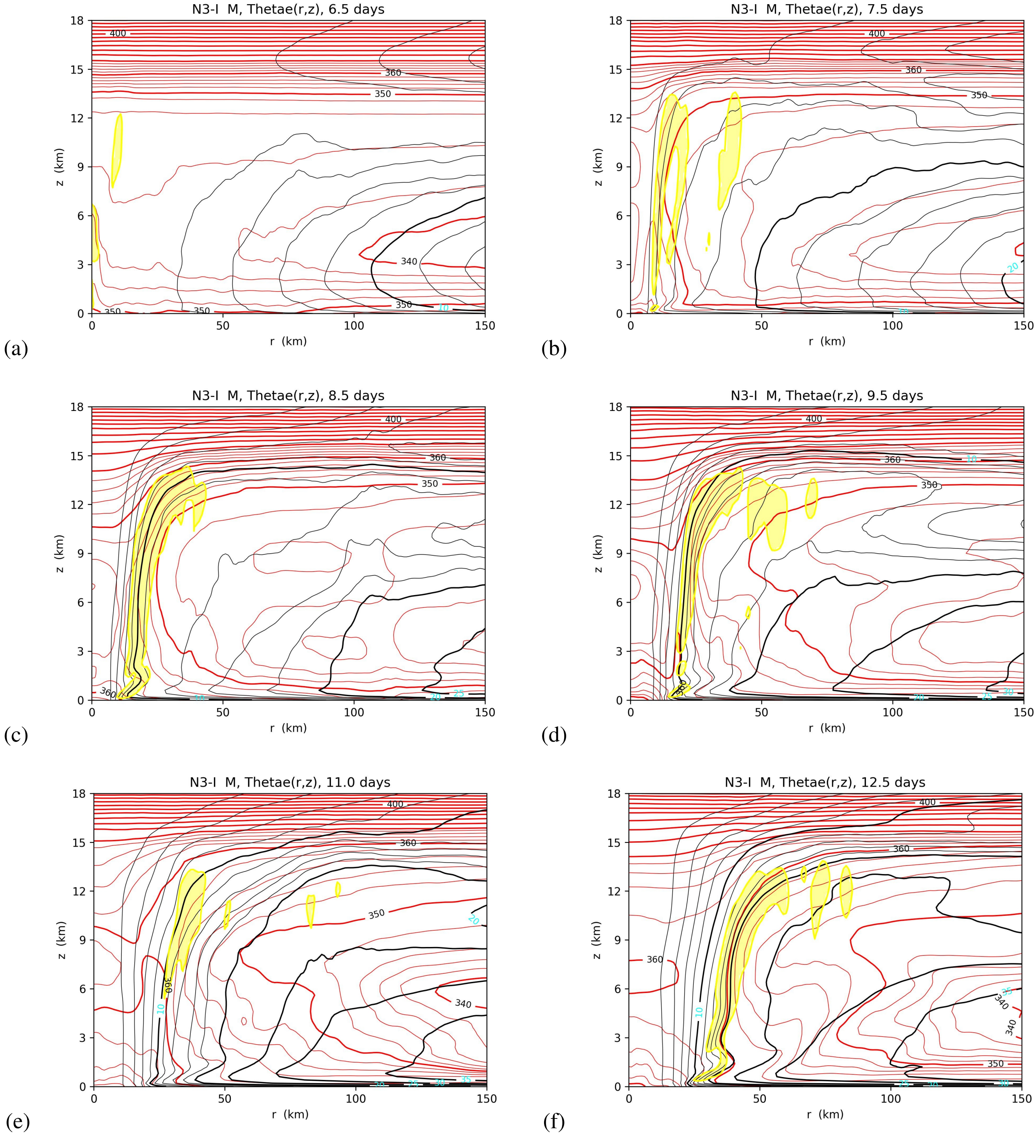

Figure 7. Radius-height cross sections of the azimuthally-averaged surfaces of θ_e and M at (a) 6.5 days, (b) 7.5 days, (c) 8.5 days, (d) 9.5 days, (e) 11 days and (f) 12.5 days from the life-cycle simulation to be discussed in Section 4. See Fig. 9 for the stage of each panel during the life cycle. Contour intervals are: θ_e (red) thick contours every 5 K, except between 340 K and 370 K where thin contours are every 2 K. Absolute angular momentum: (black) thin contours every 2×10^5 m^2 s^{-1} to 2×10^6 m^2 s^{-1}, thick contours every 1×10^6 m^2 s^{-1}. The shaded yellow region shows that of vertical velocity larger than 1 m s^{-1} and helps delineate the primary, azimuthally-averaged, cloud updraught.

flow configuration of the WISHE models typified by Fig. 6, does not appear to capture the elevated maximum of vertical velocity (and mass flux) found in both observations and numerical model simulations of developing storms (e.g., Raymond et al. 2011, Fig. 8; Lussier et al. 2014, Fig. 15; Kilroy et al. 2017, Fig. 7b,e,h,k; Montgomery and Persing 2020, Fig. 5b; Smith and Montgomery 2023, Figs. 1.4, 10.7b,d,f,h, Fig. 10.9e, Fig. 10.17a,c,e), nor, judging from Fig. 6, does it appear to capture the corresponding low-level inflow above the boundary layer (Kilroy et al. 2017, Fig. 7a,d,g; Smith and Montgomery 2023, Fig. 10.7a,c,e; Fig10.17b,d,f). The classical models do not suffer either of these limitations.

Figure 6 indicates that the overturning circulation in the WISHE models extends through the entire depth of the troposphere. Nevertheless, in the real atmosphere and in convection-permitting numerical models, the vertical extent of convection and the mass flux carried by the convection depends, inter alia, on the degree of convective instability. Thus, the ability of convection to ventilate mass converging in the frictional boundary layer of a tropical cyclone and carry this mass to the upper troposphere cannot be taken for granted (see e.g., Smith and Montgomery 2023, Section 15.5.4). If the convection is too weak, the mass fraction that cannot be ventilated will flow outwards in a shallow layer above the boundary layer leading to vortex spin down. This process is illustrated also by the classical models (Section 2.4), but will be missed entirely by the overriding assumption that $P_m \equiv 0$ globally.

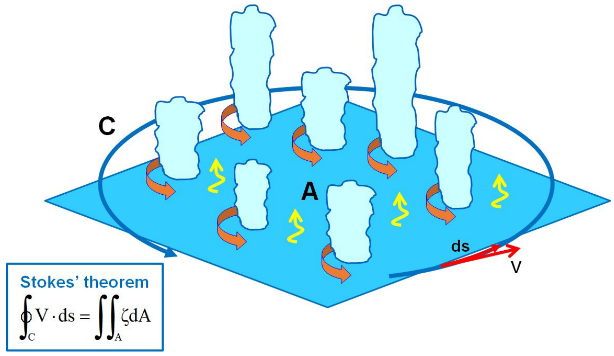

Figure 8. Schematic of a region of deep rotating updrafts, with a hypothetical horizontal circuit indicated by a circle. By Stokes' theorem, the relative circulation about the circuit is equal to the areal integral of the relative vorticity enclosed by the circuit. The yellow squiggly arrows indicate moisture fluxes from the ocean. To avoid clutter, the local and system-scale overturning circulations associated with the updraughts and downdraughts are not shown. See text for further discussion. Adapted from Smith and Montgomery (2016).

3 A three-dimensional framework

During most of the tropical cyclone life cycle, the flow is markedly asymmetric. Only near maturity is the flow approximately symmetric and even then only in the inner core region, as anticipated by the tendency of the strong differential rotation of the swirling winds to axisymmetrize convectively generated vorticity asymmetries there (e.g., Smith and Montgomery 2023, Chapter 4). Under these circumstances, the axisymmetric models discussed in Section 2 cannot be expected to apply without modification and an alternative conceptual framework is called for.

Persing et al. (2013) carried out a careful comparison between idealized simulations of tropical cyclones simulated in an axisymmetric and three-dimensional configuration, starting from the same axisymmetric initial conditions. These authors identified certain fundamental differences between vortex evolution in the two experiments as summarized in Smith and Montgomery (2023), Section 16.2. An added complication in understanding three-dimensional flows is that the material conservation of absolute angular momentum above the boundary layer cannot be assumed as there are now azimuthal pressure gradient forces to induce tangential accelerations. However a modified approach can be developed using absolute vorticity in conjunction with Stokes' theorem (Smith and Montgomery 2023, Chapter 11). This approach is described briefly below.

3.1 The rotating-convection paradigm

The dynamics of the rotating-convection paradigm are encapsulated, in part, by the azimuthal-mean tangential momentum equation, or equivalently by the vertical vorticity equation in conjunction with Stokes' theorem. Stokes' theorem equates the circulation about any fixed closed loop C to the area integral of the vorticity within that loop. Take A to be the area enclosed by loop C and the area to be in a horizontal plane, Stokes' theorem may be written in the form

$$\oint_C \mathbf{V} \cdot d\mathbf{s} = \int\int_A \zeta dA, \tag{8}$$

where $\mathbf{V}$ is the velocity vector, $d\mathbf{s}$ is a vector increment along the curve C, dA is an area element of A, and ζ is the vertical component of relative vorticity. There is a theorem by Haynes and McIntyre (1987) showing that for the circulation about the circuit C to increase, implying that the mean tangential wind about this circuit increases, vertical vorticity must be brought horizontally into the region across the boundary of C[7]. This statement is the three-dimensional analogue of the idea that for spin up, the M-surfaces have to move inwards. It turns out that the *local* enhancement of vertical vorticity by vortex-line stretching in convective updraughts totally inside C does not increase the circulation about C because the amplification of vorticity is exactly compensated by the reduced area of the enhanced vorticity.

The horizontal import of vertical vorticity into the circuit C is brought about through advection by the convergent mean overturning circulation produced by the convection within this circuit[8]. As in the axisymmetric case, the convergent mean circulation above the frictional

[7]In general, the change of horizontal circulation occurs via a line integral of a horizontal vorticity flux vector. The flux vector is the sum of an advective and non-advective component (see, e.g., Sections 2.15 and 11.1 of Smith and Montgomery 2023). For simplicity, we focus here primarily on the advective vorticity flux component.

[8]In the general case including both the advective and non-advective vorticity fluxes, the import of cyclonic vorticity by horizontal advection

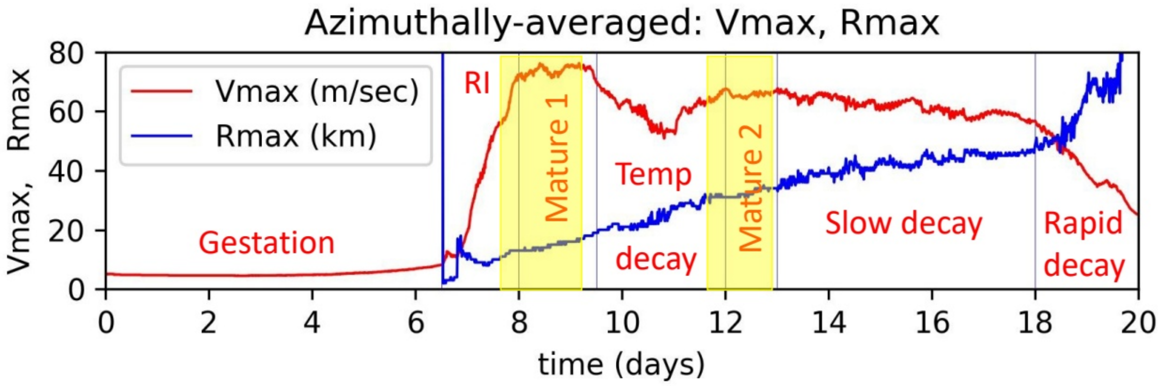

Figure 9. Time series of the maximum azimuthally-averaged tangential wind speed, Vmax (red), and the radius at which it occurs, Rmax (blue), in the tropical cyclone life cycle simulation described in the text. The figure identifies also the main periods in the life cycle including a gestation phase leading to genesis, the rapid intensification (RI) phase, a first mature phase, a period of temporary decay and re-intensification phase (Temp decay), a second mature phase, a slow decay phase and a rapid decay phase. The yellow shaded regions show approximate times during the life cycle where, *at best*, the WISHE models would be potentially applicable: see text for further discussion of this point.

boundary layer has to outweigh the mean divergent circulation there due to the boundary layer, itself, in order for it to converge net cyclonic vorticity into C. An alternative statement is that for the mean tangential wind about C to increase, the vertical mass flux being carried by the convection within C must be increasing with height to ensure, through continuity, radial inflow across, assuming of course that there is cyclonic vorticity at radii beyond C[9].

The rotating-convection paradigm is an outgrowth of the classical axisymmetric models summarized in Section 2.4, but with some important additions as discussed in Smith and Montgomery (2023), Chapter 11. *In essence, it is a collection of physical principles that provides a robust and useful framework for interpreting many aspects of tropical cyclone behaviour.* Unlike the WISHE models discussed in Section 2.5, it does not provide an analytical theory, but the physical principles on which it is based are generally applicable to understanding the complete life cycle of storms.

4 The tropical cyclone life cycle

In a recent paper, Smith et al. (2021) carried out an idealized, 20-day, cloud-permitting, three-dimensional numerical model simulation of the tropical cyclone life cycle in a quiescent environment. The life cycle begins with a period of gestation leading to genesis and ends with a period of rapid decay. The simulation starts with a relatively weak initial vortex with a maximum tangential wind speed of only 5 m s^{-1} at the surface at a radius of 200 km. This vortex is axisymmetric, cloud-free and in thermal wind balance. The thermodynamic sounding at large radius is based on the composite moist Atlantic sounding of Dunion (2011). Major features of the simulation are summarized in Chapter 15 of Smith and Montgomery (2023).

The evolution of the maximum azimuthally-averaged tangential wind speed (Vmax) from this simulation and the radius at which it occurs (Rmax) are shown in Fig. 9. The figure shows also the period where, at best, the M- and θ_e-surfaces are sufficiently congruent in the eyewall region of the vortex that the WISHE models might be conceivably invoked to explain the vortex evolution. This is notwithstanding some unrealistic aspects of these models discussed in Section 2.5.3. In contrast, Smith et al. showed that the rotating-convection paradigm provides a useful framework for understanding much of the vortex behaviour during the entire life cycle. A central idea in this framework is the appreciation that the strength of deep overturning circulation induced by deep convection and the strength of the boundary layer inflow that supplies moist air to the convection are controlled by separate processes. Specifically, the ability of deep convection to ventilate mass to the upper troposphere at the rate that mass converges in the boundary layer cannot be taken for granted (Fig. 10a).

During the genesis and rapid intensification stages of vortex evolution, the mass flux supplied by the frictional boundary layer to the inner core region of the vortex is outweighed by the mass flux carried upwards by the collective effects of deep convection (Fig. 10b). As a result, the convectively-induced inflow in the lower part of the troposphere above the frictional boundary layer is strong enough to reverse the shallow layer of outflow that would otherwise be induced by the boundary layer (see e.g., Section 2.3.3). During these stages, the boundary

occurs in combination with the generation of cyclonic vorticity (or a destruction of anticyclonic vorticity) associated with the horizontal non-advective flux within the circuit.

[9]When integrated with height from the boundary layer top, this idea forms the basis for the ventilation index introduced by Smith et al. (2021).

layer is rapidly moistened by surface evaporation, the moistening being sufficient to maintain deep convective instability. In turn, moist convection in the core leads to a moistening of the vortex core region aloft, thereby reducing the strength of convective downdraughts in the core that would otherwise act to stabilize the boundary layer to further convection.

As the vortex matures, however, the inner core boundary layer comes closer to saturation, reducing the continued flux of surface moisture supply to maintain convective instability, whereas the upper levels of the vortex warm, a natural consequence of balance dynamics (e.g., Smith and Montgomery (2023), Section 5.3). The upper-level warming has a stabilizing effect on inner-core deep convection and gradually gains the upper hand. As a result, the collective effects of deep convection become progressively less able to ventilate mass at the rate that mass is supplied by the boundary layer. This inability is enhanced by the increase in the boundary-layer mass flux as the vortex intensifies and broadens. The broadening is reflected, in part, by the progressive increase in the radius of maximum tangential wind speed shown in Fig. 9 as well as the increase in the radius of gales (see Smith et al. 2021, Fig. 1c). The broadening is, itself, a consequence of continued lower-tropospheric inflow above the boundary layer. Eventually, a situation is reached where convection is no longer able to ventilate all the mass converging in the boundary layer and the fraction that cannot be ventilated flows outwards in a shallow layer above the boundary layer (Fig. 10c). When this happens, the tangential wind spins down locally, as in the friction only calculation discussed in Section 2.3.3, and the boundary layer flow weakens in response.

In the Smith et al. simulation, the processes described above account also for the temporary decay and subsequent re-intensification of the vortex between about $9\frac{1}{2}$ and 12 days. The decay is accompanied by a weakening of the mass flux carried by the inner eyewall convection and the resulting low-level outflow triggers a band of deep convection at larger radii. Subsequently, a new eyewall cloud forms at a larger radius than the original eyewall, but inside the band of deep convection. The re-intensification is accompanied by this new eyewall formation and the convection beyond it progressively decays.

The foregoing processes are broadly analogous to reducing the bubbling rate in the Turner-Lilly bubbling experiment, suitably modified for tropical cyclones as described in Section 2.2.1. One could imagine first reducing the bubbling rate from a ring of bubbling tubes and then increasing the rate while increasing the radius of the bubbling tubes. The additional effect in the foregoing numerical simulation is the stable stratification of the model atmosphere, which confines the unventilated radial outflow from the boundary layer to a shallow layer just above the boundary layer.

As time proceeds in the life-cycle simulation, the same sequence of events accounts for the slow decay from about 13 to 18 days. The rapid decay after 18 days is accompanied by the rapid collapse of any deep convection and the occurrence of radial outflow through the entire troposphere.

Referring to the time series of Vmax in Fig. 9, it is clear from the ventilation ideas encapsulated in Fig. 10 that rapid intensification would take place in conditions where the deep convective mass flux averaged over the inner-core region significantly exceeds the rate at which mass is supplied to this region by the boundary layer. These conditions would lead to the largest inflow velocity above the boundary layer and thereby the largest inward advection of the M-surfaces. Thus, there is no intrinsic difference in the physical mechanisms involved between intensification and rapid intensification, only the relative magnitudes of the key processes. Recognition of this fact would seem to offer the potential for the construction of a simple diagnostic tool derivable from forecast models that could help to anticipate periods of rapid intensification, such as the ventilation parameter introduced in Section 15.5.4 of Smith and Montgomery (2023).

4.1 Applicability of WISHE models?

While the rotating-convection paradigm provides a framework for interpreting the physics of vortex evolution in the foregoing life-cycle simulation, the individual processes involved are coupled nonlinearly and it is not possible to isolate them: one is forced to solve the problem numerically. The processes leading to spin up during the period of rapid intensification are essentially those captured by the classical models summarized in Section 2.4: i.e., vortex spin up is principally a result of the inward advection of the azimuthally-averaged M-surfaces in the lower tropospheric branch of the overturning circulation above the frictional boundary layer where the azimuthally-averaged M is approximately materially conserved. These processes, in conjunction with the accompanying boundary layer dynamics and thermodynamics, account also for the tendency of the azimuthally-averaged M- and θ_e-surfaces to become approximately congruent as the vortex matures. This tendency would be expected if air parcels rising into the eyewall approximately conserve the values of M and θ_e with which they left the boundary layer. Obviously, in regions where the air is saturated at every azimumth, the θ_e-surfaces will coincide with those of θ_e^*. However, if ice processes are modelled, pseudo-adiabatic θ_e conservation cannot be assumed when the clouds glaciate in the upper troposphere.

It would seem to be against causality to postulate that, when a sufficient degree of congruence between M and θ_e is achieved in the eyewall, this congruence becomes the key constraint *globally* and the material

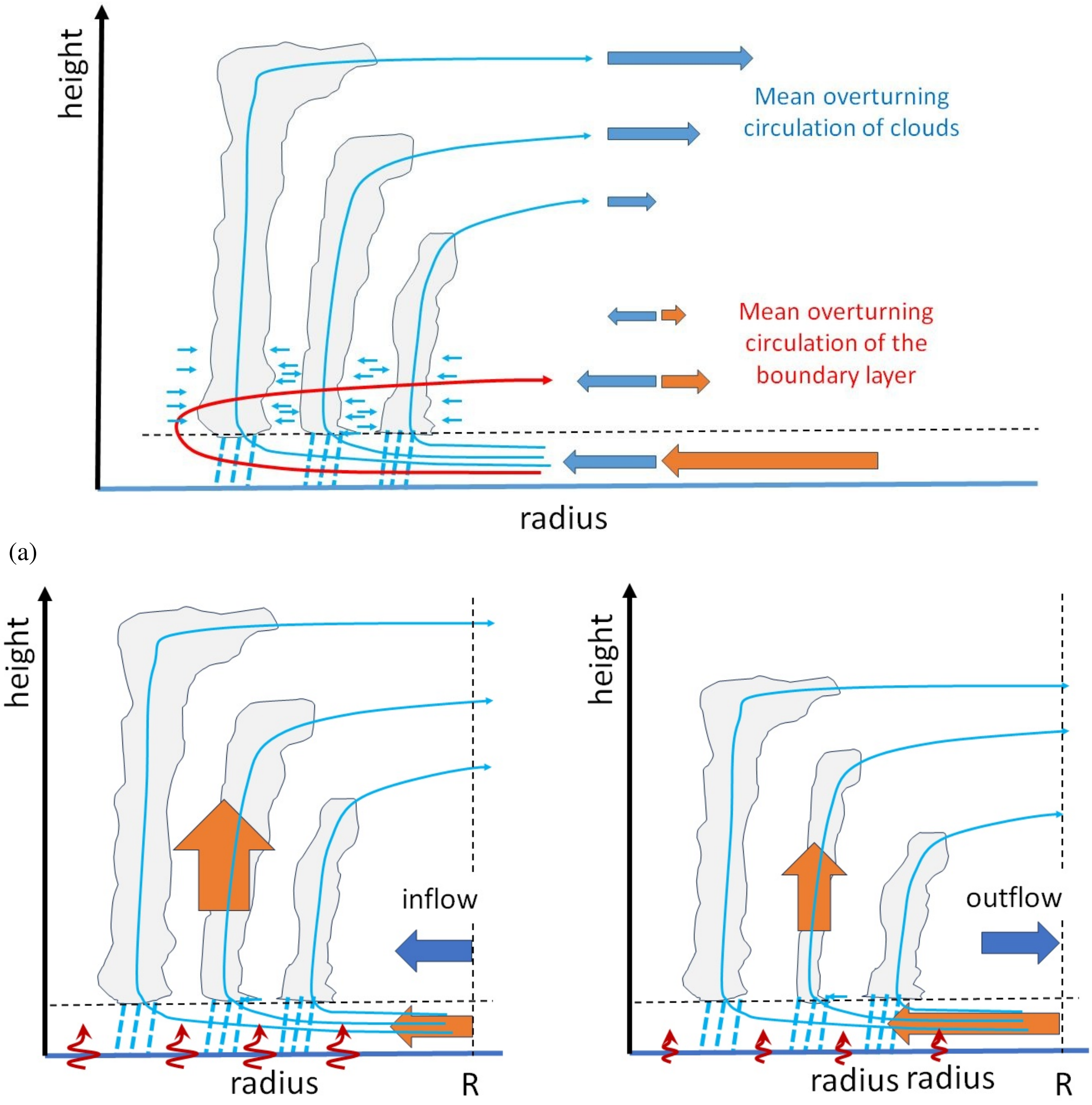

(a)

(b) (c)

Figure 10. (a) Depiction of the azimuthally-averaged overturning circulations induced by deep convection (in blue) and by the frictional boundary layer (in red). The collective effects of deep convection is to produce inflow in the lower troposphere, above and within the frictional boundary layer, in part by entrainment. The boundary layer top is indicated by the thin horizontal dashed line. In contrast, the boundary layer leads to inflow within it and outflow in a shallow layer above it as exemplified by the balance calculation in Fig. 5. The ability of deep convection to ventilate mass to the upper troposphere at the rate mass converges in the boundary layer cannot be taken for granted. In general, there are two scenarios illustrated in (b) and (c). In these panels, the green curvy arrows symbolize surface enthalpy fluxes, which are largest in the intensification stage of development. In (b), the net upward mass flux carried by convection in a cylindrical region of radius R exceeds the mass flux entering this cylinder in the boundary layer, whereupon, through continuity, there must be inflow in the lower troposphere above the boundary layer. This situation is most pronounced in the genesis and rapid intensification phases of the vortex life cycle. It is the inflow above the boundary layer that draws absolute momentum surfaces inwards leading to spin up. In (c), the mass flux entering this cylinder in the boundary layer exceeds the net upward mass flux carried by deep convection leading to outflow in the lower troposphere above the boundary layer. This situation becomes progressively established in the mature and decay phases of the vortex life cycle. The outflow above the boundary layer carries absolute momentum surfaces outwards leading to spin down above the boundary layer.

conservation of M above the boundary layer can be dispensed with (cf. Subsection 2.5.1). This would seem to be exactly what the WISHE models are doing to build a theory for the subsequent evolution of the vortex. It is the authors' view that, despite the mathematical elegance of these models, they are of questionable utility for understanding most, if not all aspects of the tropical cyclone life cycle.

5 Conclusions

We have examined possible conceptual frameworks, both axisymmetric and three-dimensional, for understanding the physics of the tropical cyclone life cycle in an idealized, three-dimensional, numerical simulation in a quiescent environment. We suggest that an essential element of any axisymmetric framework should be the assumption that absolute angular momentum is materially conserved above the frictional boundary layer. Such conservation implies that vortex spin up requires radial inflow above the friction layer, while radial outflow there leads to spin down. We showed that, with this assumption, many aspects of vortex behaviour in an axisymmetric framework may be illustrated by two simple laboratory experiments.

We noted that, in the widely popular axisymmetric WISHE models, the material conservation of absolute angular momentum is disregarded in favour of assuming that the saturated moist equivalent potential vorticity is everywhere zero, or equivalently that the surfaces of absolute angular momentum and saturation moist equivalent potential temperature (or, equivalently, saturation moist entropy) are congruent globally at all times. Evidence is presented showing that, at best, this assumption would limit the applicability of the WISHE models to a small fraction of the tropical cyclone life cycle. However, our analysis of a recent three-dimensional numerical simulation examining the tropical cyclone life cycle unveils a causality problem with assuming that global congruence controls vortex evolution. In particular, dispensing with the implementation of the material conservation of absolute angular momentum allows for the occurrence of sources or sinks of this quantity and these may be nonphysical.

Because of differences in behaviour between the dynamics of convective rings and locally rotating-convective updraughts, the three-dimensional framework is ultimately the proper framework for understanding the tropical cyclone life cycle. We showed that, in this framework, the rotating-convection paradigm provides an understanding of much of the vortex behaviour during the tropical cyclone life cycle. Like the classical Eliassen model, it highlights the importance for vortex spin up of the deep, convectively-induced overturning circulation being strong enough to generate inflow above the frictional boundary layer in the presence of the ubiquitous tendency of the boundary layer to generate outflow there. When deep convection is too weak to ventilate all the mass that is converging in the boundary layer to the upper troposphere, there is net outflow above the boundary layer and the vortex weakens. This behaviour appears to be ruled out in the WISHE models by their overriding assumption of global moist neutrality, but is a feature of the classical Eliassen model.

Finally, the ventilation ideas discussed in Section 4 suggest that there is no intrinsic difference in the dynamics of tropical cyclone intensification and that of rapid intensification. Moreover, we pointed out that these ideas offer potential for the construction of a diagnostic tool derivable from forecast models that could help to anticipate periods of rapid intensification.

Acknowledgements

We thank Michael Reeder and an anonymous reviewer for their perceptive comments on the first version of the manuscript. The views expressed herein are those of the authors and do not represent sponsoring agencies or institutions.

References

Bui, H. H., R. K. Smith, M. T. Montgomery, and J. Peng, 2009: Balanced and unbalanced aspects of tropical-cyclone intensification. *Quart. Journ. Roy. Meteor. Soc.*, **135**, 1715–1731.

Dunion, J. P., 2011: Rewriting the climatology of the tropical north atlantic and caribbean sea atmosphere. *J. Clim.*, **24**, 893–908.

Eliassen, A., 1951: Slow thermally or frictionally controlled meridional circulation in a circular vortex. *Astrophys. Norv.*, **5**, 19–60.

Eliassen, A., 1962: On the vertical circulations in frontal zones. *Geofys. Publ.*, **24**, 147–160.

Emanuel, K. A., 1989: The finite-amplitude nature of tropical cyclogenesis. *J. Atmos. Sci.*, **46**, 3431–3456.

Emanuel, K. A., 1995: The behavior of a simple hurricane model using a convective scheme based on subcloud-layer entropy equilibrium. *J. Atmos. Sci.*, **52**, 3960–3968.

Emanuel, K. A., 1997: Some aspects of hurricane inner-core dynamics and energetics. *J. Atmos. Sci.*, **54**, 1014–1026.

Emanuel, K. A., 2000: *Quasi-equilibrium thinking, In: General Circulation Model Development, Ed. D. A. Randall*. Academic Press, NewYork, 225–255 pp.

Emanuel, K. A., 2012: Self-stratification of tropical cyclone outflow. Part II: Implications for storm intensification. *J. Atmos. Sci.*, **69**, 988–996.

Haynes, P., and M. E. McIntyre, 1987: On the evolution of vorticity and potential vorticity in the presence of diabatic heating and frictional or other forces. *J. Atmos. Sci.*, **44**, 828–841.

Kilroy, G., R. K. Smith, and M. T. Montgomery, 2017: A unified view of tropical cyclogenesis and intensification. *Quart. Journ. Roy. Meteor. Soc.*, **143**, 450–462.

Lussier, L., M. T. Montgomery, and M. M. Bell, 2014: The genesis of Typhoon Nuri as observed during the Tropical Cyclone Structure 2008 (TCS-08) field experiment - Part 3: Dynamics of low-level spin-up during the genesis. *Atmos. Chem. Phys.*, **14**, 8795–8812.

Montgomery, M. T., M. E. Nichols, T. A. Cram, and A. B. Saunders, 2006: A vortical hot tower route to tropical cyclogenesis. *J. Atmos. Sci.*, **63**, 355–386.

Montgomery, M. T., and J. Persing, 2020: Does balance dynamics well capture the secondary circulation and spinup of a simulated hurricane? *J. Atmos. Sci.*, **78**, 75–95.

Morton, B. R., 1966: *Geophysical vortices, In Prog. In Aeronautical Sci., Ed. Küchemann*, Vol. 7. Pergamon, 145-194 pp.

Ooyama, K. V., 1982: Conceptual evolution of the theory and modeling of the tropical cyclone. *J. Meteor. Soc. Japan*, **60**, 369–380.

Persing, J., M. T. Montgomery, J. McWilliams, and R. K. Smith, 2013: Asymmetric and axisymmetric dynamics of tropical cyclones. *Atmos. Chem. Phys.*, **13**, 12 299–12 341.

Raymond, D. J., S. Sessions, and C. Lopez-Carillo, 2011: Thermodynamics of tropical cyclogenesis in the northwest Pacific. *J. Geophys. Research*, **116**, 1–18.

Schubert, W. H., and B. T. Alworth, 1982: Evolution of potential vorticity in tropical cyclones. *Quart. Journ. Roy. Meteor. Soc.*, **39**, 1687–1697.

Schubert, W. H., and J. J. Hack, 1982: Inertial stability and tropical cyclone development. *J. Atmos. Sci.*, **39**, 1687–1697.

Schubert, W. H., and J. J. Hack, 1983: Transformed Eliassen balanced vortex model. *J. Atmos. Sci.*, **40**, 1571–1583.

Shapiro, L. J., and H. Willoughby, 1982: The response of balanced hurricanes to local sources of heat and momentum. *J. Atmos. Sci.*, **39**, 378–394.

Smith, R. K., G. Kilroy, and M. T. Montgomery, 2014: Why do model tropical cyclones intensify more rapidly at low latitudes? *J. Atmos. Sci.*, **140**, 1783–1804.

Smith, R. K., G. Kilroy, and M. T. Montgomery, 2021: Tropical cyclone life cycle in a three-dimensional numerical simulation. *Quart. Journ. Roy. Meteor. Soc.*, **147**, 3373–3393.

Smith, R. K., and L. M. Leslie, 1976: Thermally driven vortices: a numerical study with application to dust devils. *Quart. Journ. Roy. Meteor. Soc.*, **102**, 791–804.

Smith, R. K., and M. T. Montgomery, 2016: Understanding hurricanes. *Weather*, **71**, 219–223.

Smith, R. K., and M. T. Montgomery, 2023: *Tropical cyclones: Observations and basic processes*. Elsevier, London, 411pp.

Smith, R. K., M. T. Montgomery, and H. Bui, 2018: Axisymmetric balance dynamics of tropical cyclone intensification and its breakdown revisited. *J. Atmos. Sci.*, **75**, 3169–3189.

Smith, R. K., M. T. Montgomery, and S. Wang, 2024: Can one reconcile the classical theories and the WISHE-theories of tropical cyclone intensification? *Tropical Cyclone Research and Review*, **13**, In review.

Turner, J. S., and D. K. Lilly, 1963: The carbonated-water tornado vortex. *Quart. Journ. Roy. Meteor. Soc.*, **20**, 468–471.

Črnivec, N., R. K. Smith, and G. Kilroy, 2015: Dependence of tropical cyclone intensification rate on sea surface temperature. *Quart. Journ. Roy. Meteor. Soc.*, **140**, 1618–1627.

Wang, S., M. T. Montgomery, and R. K. Smith, 2021: Solutions of the Eliassen balance equation for inertially and/or symmetrically stable and unstable vortices. *Quart. Journ. Roy. Meteor. Soc.*, **145**, 2760–2771.

Wang, S., and R. K. Smith, 2019: Consequences of regularizing the Sawyer-Eliassen equation in balance models for tropical cyclone behaviour. *Quart. Journ. Roy. Meteor. Soc.*, **145**, 3766–3779.

Willoughby, H. E., 1979: Forced secondary circulations in hurricanes. *J. Geophys. Res.*, **84**, 3173–3183.

Zhang, J. A., D. S. Nolan, R. F. Rogers, and V. Tallapragada, 2015: Evaluating the impact of improvments in the boundary layer parameterization on hurricane intensity and structure forecasts in HWRF. *Mon. Wea. Rev.*, **143**, 3136 – 3155.

Zhu, P., A. Hazelton, Z. Zhang, F. D. Marks, and V. Tallapragada, 2021: The role of eyewall turbulent transport in the pathway to intensification of tropical cyclones. *J. Geophys. Res. Atmospheres*, **126**, 1–26.